Tuning the Reduction Potential of Engineered Cytochrome *c*-553[†]

Andrea Fantuzzi,[‡] Sheila Sadeghi,[‡] Francesca Valetti,[‡] Gian Luigi Rossi,[§] and Gianfranco Gilardi*,[‡]

Department of Biological Sciences, Biochemistry Building, Imperial College of Science, Technology, and Medicine, London SW7 2AY, U.K., and Department of Biochemistry and Molecular Biology, University of Parma, 43100 Parma, Italy

Received March 1, 2002; Revised Manuscript Received May 14, 2002

ABSTRACT: Cytochrome *c*-553 from *Desulfovibrio vulgaris* exhibits a highly exposed heme and an unusually low reduction potential with respect to other *c*-type cytochromes. Solvent heme exposure has been indicated as one of the most important factors in modulating the midpoint potential of the redox center. To test this hypothesis, a unique surface-exposed cysteine has been substituted for either M23 or G51 to produce the corresponding mutants and allow the formation of homodimers through a specific disulfide bridge. The reduction potentials, determined via spectroelectrochemistry, show an increase from +20 ± 5 mV for the wt to +88 ± 5 and +105 ± 5 mV for the M23C−M23C homodimer and G51C−G51C homodimer, respectively. Chemical denaturation of the homodimers leads to parameters related to the hydrophobicity (*m*) and the number of buried side chains (n_B), which suggest a decrease of exposure of the heme as a result of dimerization. These results are consistent with the heme-accessible surface area (ASA) calculated from a computer model of the homodimers. The ASA values show a decrease from 73 Å^2 for the wt to 66 and 50 Å^2 per heme for the M23C−M23C homodimer and G51C−G51C homodimer, respectively. The trend of the *m*- and n_B-values, the degree of solvent accessibility, and the midpoint potential observed upon formation of the homodimers indicate a correlation between the reduction potential values and the exclusion of water from the heme surface.

Tuning of the reduction potential of heme by the protein matrix is important in the regulation of biological electron transfer (*1*−*3*). While substitution of different axial ligands to the heme of *c*-type cytochromes may shift the reduction potential by as much as 150 mV, hemes with the same axial ligands exhibit reduction potentials varying in a range of 300 mV, depending on the protein environment (*4*−*6*). In a systematic study of *different c*-type cytochromes Gray and co-workers have shown that the reduction potential can vary by as much as 500 mV depending on the level of heme exposure to solvent (*7*). This work reports on the use of the *same* molecule to test the correlation between heme exposure and reduction potential.

Cytochrome *c*-553 (cyt *c*-553)[1] from *Desulfovibrio vulgaris* Hildenborough exhibits an abnormally low reduction potential: in the case of the recombinant protein it has been determined by spectroelectrochemistry to be +20 ± 5 mV (this work) or +37 ± 5 mV (*8*). A comparative study of the accessible surface area (ASA) of the heme of *c*-553 with that of other cytochromes *c* that exhibit high reduction potentials shows that the ASA of *c*-553 is higher. This high exposure of the heme might be responsible for its unusually low reduction potential (*9*). The analysis of the temperature dependence of the reduction potentials of cytochrome *c*-553 from *D. vulgaris* Hildenborough (*8*) and *Bacillus pasteurii* (*10*) and the comparison with other cytochromes show an entropic contribution due to solvent ordering at the exposed heme. Therefore, this cytochrome seems a good model to test the possibility of tuning the reduction potential toward the higher values characteristic of other cytochromes of the same class and similar structure by decreasing the heme ASA. This cytochrome is rather unique, sharing only 13% sequence homology with tuna cytochrome *c* and 26% homology with the similarly sized cyt *c*-551 from *Pseudomonas aeruginosa*. It is a member of class Ib of cytochromes *c*, characterized by the covalent attachment of the *c*-type heme at two cysteine residues and by His and Met ligation of the heme iron.

The NMR structure of the reduced cytochrome *c*-553 from *D. vulgaris* Hildenborough strain (DvH) has been determined (*9*), and the analysis of structure and dynamics (*11*) shows that the ensemble of the final 36 structures can be separated into two subfamilies, F1 (12 members) and F2 (24 members), depending on the structure of the motif Gly50/Arg53 and the hydrogen-bonding network in the heme region (*11*). Constraint-free molecular dynamics shows that Gly50 is unable to retain the starting backbone conformation and indicates a large mobility for the Ω-loop (Gly 24) and the Gly47−Arg53 motif (*11*). The comparison of the two subfamilies shows a structural heterogeneity resulting in a rearrangment of the local structure at the heme's propionate-

[†]This work was supported by HFSP Grant RG-44/98 and EC Grant BIO CT960413. G.L.R. acknowledges the MIUR and the CNR (Target Project on Biotechnology) of Italy for financial support.

* To whom correspondence should be addressed. Tel: ++44 20 75945320. Fax: ++44 20 75945330. E-mail: g.gilardi@ic.ac.uk.

[‡] Imperial College of Science, Technology, and Medicine.

[§] University of Parma.

[1] Abbreviations: ASA, accessible surface area; CD, circular dichroism; CV, cyclic voltammetry; cyt *c*-553, cytochrome *c*-553; ΔΘ, difference in molar ellipticity; K_U, denaturation equilibrium constant; f_U, fraction of unfolded protein; f_N, fraction of native protein; Δ*G*, Gibbs free energy difference; $\Delta G_{s,m}$, maximum unfolding solvation free energy at infinite denaturant concentration; [GuHCl], molar concentration of guanidinium chloride; NHE, normal hydrogen electrode; *E*, reduction potential; E_m, midpoint potential; *F*, Faraday constant; *m*-value, molar cosolvent term; n_B-value, number of buried side chains that become exposed on denaturation; N, native protein; U, unfolded protein; wt, wild type.

10.1021/bi025759x CCC: $22.00
Published on Web 06/14/2002

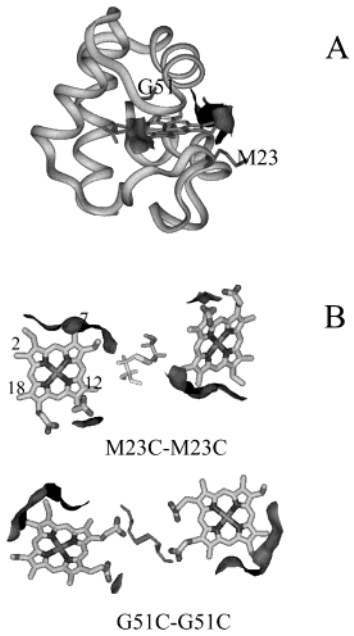

FIGURE 1: (A) α-Carbon ribbon representation of the structure of cytochrome *c*-553. Residues M23, G51, and the heme are rendered as stick representation. The heme-accessible surface area, calculated according to the Connolly algorithm, is shown. (B) M23C−M23C and G51C−G51C homodimers of *c*-553. For clarity, only the hemes and the disulfide bonds are shown. The heme-accessible surface is represented. The numbers refer to the heme methyl groups.

6/solvent interface. The solvent exposure of this propionate is rather unique within the cytochromes of known structure; furthermore, its hydrogen-bonding pattern is different in the two subfamilies while its solvent accessibility is greater in F2 than in F1.

All the characteristics reported above, namely, the unusually low reduction potential, the solvent exposure of the heme, and the flexibility of the protein matrix shown by NMR, underline the suitability of cyt *c*-553 as a candidate for a study on the influence of these factors in tuning the reduction potential.

Is it possible to engineer cyt *c*-553 in such a manner that its reduction potential reaches the level of the other cytochromes? To answer this question, two surface-exposed residues, either Gly51 or Met23, were substituted by a cysteine to allow for dimer formation through a disulfide bridge. The two mutation sites were chosen in the regions that distinguish the two subfamilies because of their flexibility and because they are proximal to the exposed heme edges. This paper reports on the construction and functional characterization of two *c*-553 homodimers, M23C−M23C and G51C−G51C, engineered in the Ω-loop and Gly47−Arg53 motif, respectively (Figure 1).

EXPERIMENTAL PROCEDURES

Mutant Engineering and Protein Purification. Wild-type cytochrome *c*-553 has been expressed and purified as previously described (*12*). The cysteine mutants were constructed in the expression plasmid pJRC41 (*13*) using a two-step PCR. The mutagenic oligonucleotides 5′-TCCAAGGCTGCCTGTGGTTCGGCC-3′ and 5′-TCCTACGGTTGCGAGCGCAAGGCC-3′ were used for constructing the Met23 → Cys and the Gly51 → Cys mutants, respectively. The mutations were confirmed by DNA sequencing.

The G51C and M23C mutants were purified using SP-Sepharose (Pharmacia, 30 cm × 2.5 cm) using a 5 mM potassium phosphate buffer, pH 6.0, and 2 mM dithiothreitol (DTT) and eluted with a linear gradient of 0−150 mM NaCl, followed by a Sephadex G-50 column (Pharmacia, 90 cm × 2 cm) with a 5 mM potassium phosphate buffer, pH 6.0, and 2 mM DTT. The purity was estimated as described in ref *12*.

Dimerization. Dimerization of the two cysteine mutants was obtained by concentrating the sample of the monomers to 50−100 μM in 5 mM potassium phosphate, pH 6.0, overnight at 4 °C. Under these conditions the yield of homodimers was around 80% of the total protein. The *c*-553 homodimers were separated from the monomers by SP−Sepharose chromatography. The purity of the sample and the dimer/monomer ratio were estimated on a silver-stained Homogeneous 20 Pharmacia precasted gel for SDS−PAGE run in the absence of β-mercaptoethanol.

Spectroscopic Characterization. CD spectra were collected at 25 °C with a Jasco 600 spectropolarimeter. The protein concentration was 0.15 mg/mL for the wt and 0.20 mg/mL for the two homodimers in 50 mM potassium phosphate, pH 6.0.

^{1}H NMR experiments were carried out on 1.2 mM and 80 μM samples for the wt and the dimers, respectively. Samples were prepared in 10% D_2O in 0.1 M potassium phosphate buffer, pH 5.9. ^{1}H NMR spectra were recorded at 37 °C in a Fourier mode on a Bruker AMX 500 spectrometer. Chemical shifts were determined using tetramethylsilane as internal standard.

Cyclic Voltammetry. Cyclic voltammograms were measured at 25 °C with an Autolab 10 potentiostat controlled by the GPES software (Eco Chemie, Utrecht, The Netherlands). The electrochemical experiments were performed with a three-electrode cell using the method described by Hagen (*14*). The working electrode was a glassy carbon disk activated with nitric acid; platinum wire was used as the counter electrode, and a saturated calomel electrode (Radiometer) was used as the reference. All potential values are reported with respect to the normal hydrogen electrode (NHE). The protein concentration was 1 mg/mL in 50 mM potassium phosphate, pH 7.5.

Potentiometric Titration. Potentiometric titrations were performed in an anaerobic cuvette equipped with a platinum working electrode and an Ag/AgCl reference electrode (*15*). Ambient reduction potentials were adjusted by addition of aliquots (2−5 μL) of sodium dithionite (0.1 mM) or potassium ferricyanide (0.1 mM). Titrations were performed in 50 mM potassium phosphate, pH 7.5. Electrode−solution mediation was facilitated by the following mediators at 1−5 μM concentration: phenazine methosulfate ($E_m = +80$ mV), methylene blue ($E_m = +11$ mV), resorufin ($E_m = -51$ mV), and 1,2-naphthoquinone ($E_m = -145$ mV). The modified cuvette was flushed with oxygen-free nitrogen before and during the measurements. After equilibration at each potential, the optical spectrum was recorded. Reduction of the heme in cytochrome *c*-553 was followed by the increase in the α-band absorption at 553 nm, where the absorption of the mediators was negligible compared to that of the protein, using a Hewlett-Packard 8452 diode array spectrophotometer. The fraction of reduced heme, proportional to the spectral intensity, was plotted against potential, and the data were

fit to a single Nernst equation with the fitting parameter n free to float:

$$E = E_m + (RT/nF) \ln([ox]/[red]) \quad (1)$$

where [ox] and [red] are the concentrations of oxidized and reduced heme, respectively, E is the solution reduction potential at equilibrium, n is the number of electrons, E_m is the midpoint potential in the conditions given above, F is the Faraday constant, R is the gas constant, and T is the absolute temperature.

Protein Denaturation. CD spectra were recorded on a Jasco-720 spectropolarimeter using a 1 mm thick cell, thermostated at 25 °C. The GuHCl titrations of the oxidized cytochrome *c*-553 wt and mutants (2 μM) were performed in 50 mM potassium phosphate buffer, pH 7.5. Protein unfolding was shown to be reversible. In each experiment, denaturation of the protein was reached within less than 1 min. The experimental data were analyzed by assuming a two-state model N ↔ U. Given that f_N and f_U represent the fraction of total protein in the native and unfolded state, respectively ($f_N + f_U = 1$), the equilibrium constant K_U and the free energy change $\Delta G_{obs}{}^U$ for the unfolding reaction were calculated from

$$K_U = f_U/(1 - f_U) = f_U/f_N \quad (2)$$

$$\Delta G_{obs}{}^U = -RT \ln K_U \quad (3)$$

According to the linear extrapolation method (*16*), the unfolding free energy depends linearly on the denaturant concentration:

$$\Delta G_{obs}{}^U = \Delta G_{obs}{}^{H_2O} - m[\text{GuHCl}] \quad (4)$$

where m is the molar cosolvent term, $\Delta G_{obs}{}^{H_2O}$ is the extrapolated value to 0 [GuHCl] of the difference in free energy, and [GuHCl] is the concentration of denaturant.

Experimental data were fitted using an equation that merges the above equations (*17*):

$$\Delta\Theta = \{[(\Delta\Theta_N + m_N[\text{GuHCl}]) + (\Delta\Theta_U + m_U[\text{GuHCl}])] \exp\{-[(\Delta G_{obs}{}^{H_2O} + m[\text{GuHCl}])/RT]\}\}/\{1 + \exp\{-[(\Delta G_{obs}{}^{H_2O} + m[\text{GuHCl}])/RT]\}\} \quad (5)$$

where $\Delta\Theta$ is the difference in molar ellipticity measured at 218 nm, [GuHCl] is the concentration of denaturant, R is the gas constant, T is the absolute temperature, and $\Delta\Theta_N$, $\Delta\Theta_U$, m_N, m_U, m, and $\Delta G_{obs}{}^{H_2O}$ are fitting parameters.

The unfolding process has also been analyzed according to Staniforth et al. (*18*) using the equation:

$$\Delta G_{obs} = \Delta G_{obs}{}^{H_2O} - n_B \Delta G_{s,m}[\text{GuHCl}]/(K_{DEN} + [\text{GuHCl}]) \quad (6)$$

where n_B is the number of buried side chains that become exposed to solvent on unfolding (*18*), $\Delta G_{s,m}$ represents the maximum unfolding solvation free energy at infinite denaturant concentration (3.24 kJ/mol in GuHCl), and K_{DEN} is an empirical constant that represents the concentration of denaturant at which half $\Delta G_{s,m}$ is reached (with a value of 5.4 M in GuHCl). Both K_{DEN} and $\Delta G_{s,m}$ are constants determined for the buried side chains in an average protein (*18*).

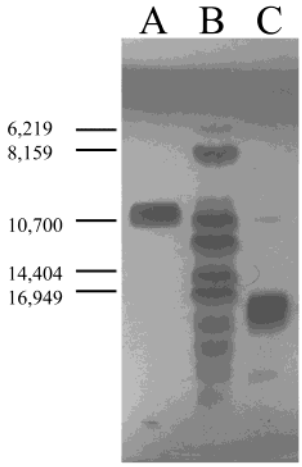

FIGURE 2: Silver-stained SDS−PAGE (20% acrylamide, no β-mercaptoethanol) of the cytochrome *c*-553 M23C monomer (lane A) and dimer (lane C). Lane B shows the molecular weight markers (horse myoglobin peptides) as listed on the left.

RESULTS AND DISCUSSION

Dimerization of the purified mutants leads to pure dimeric species as shown in Figure 2. The UV−vis absorption spectra of the oxidized wild-type *c*-553 (wt) and the M23C−M23C and G51C−G51C homodimers show that the peak position in the visible region is unaffected by dimerization while the molar extinction coefficient of the γ-band is slightly higher when spectra are normalized at 280 nm.

Both CD and NMR (heme region) spectroscopy were used to investigate whether dimerization had affected the tertiary or secondary structure of the cytochrome. The far-UV and near-UV−vis CD spectra of cyt *c*-553 wt and homodimers are shown in Figure 3. No differences are observed in the far-UV region, suggesting that the secondary structure content of the wt is preserved in the engineered molecules. In the near-UV region, the intense heme absorption prevails over the intrinsic protein absorption and prevents CD analysis of the protein tertiary structure. The visible (heme) region shows a splitting of the Soret band typical of several cytochromes *c*, which is correlated with the influence of the protein matrix on the $\pi-\pi^*$ electronic transition. Dimerization does not induce alterations of the shape of the band while minor differences in intensity are consistent with the changes in molar extinction coefficient. These results indicate that the homodimers are folded and that the secondary and tertiary structures of the mutants are similar to those of the wt protein.

To support this evidence, NMR spectroscopy was used to probe the tertiary structural integrity, with particular reference to the heme region. Proton NMR spectra were collected for the wt protein and the homodimers under identical experimental conditions. The presence of sharp resonances and the identical chemical shift of peaks in the upfield region confirm that the monomers both in isolation and within the homodimers are folded. The comparison between the NMR spectra of the M23C−M23C and G51C−G51C dimers and that of the wt monomer (*19*) showed the occurrence of broader peaks in the former ones, consistent with the presence of higher molecular weight species. Close inspection of the heme region allowed assignment of most of the heme

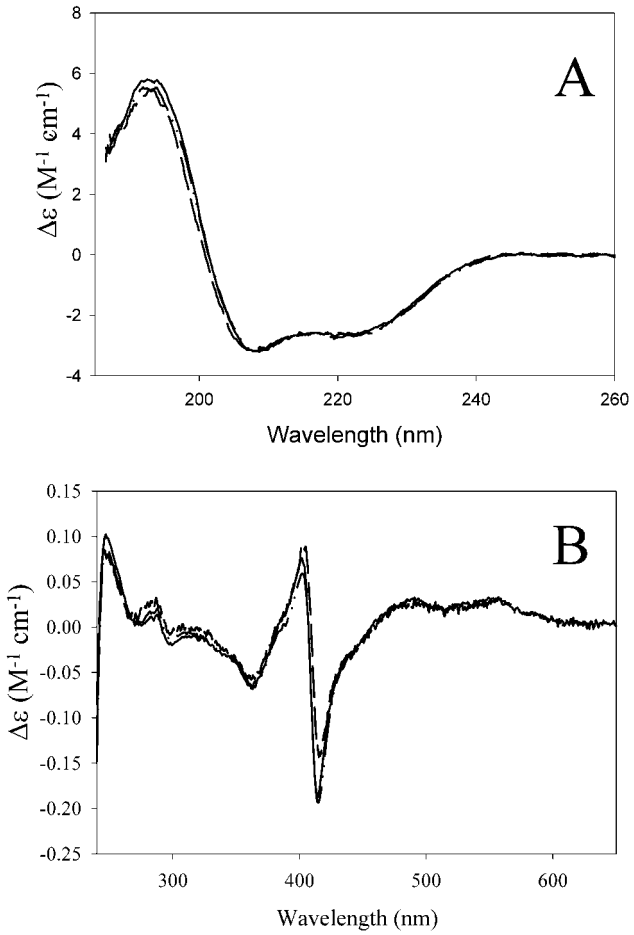

FIGURE 3: CD spectra of cytochrome *c*-553. Far-UV (A) and near-UV and visible (B) regions: wt (−••−), M23C−M23C dimer (− −), and G51C−G51C dimer (−).

resonances. Some small differences were observed: the M23C−M23C and G51C−G51C dimers showed a shift in the heme methyl resonances associated with Me2 (20.8 ppm for wt; 21.2 ppm for M23C−M23C; 20.2 ppm for G51C−G51C), Me7 (23.2, 23.4 ppm for wt; 23.0, 23.2 ppm for M23C−M23C; 22.7, 23.0 ppm for G51C−G51C), and Me12 (22.3 ppm for wt; 22.4, 22.6 ppm for M23C−M23C; 21.8 ppm for G51C−G51C) where Me7 and Me12 are close to both of the mutation sites. These differences are probably due to the heme protons sensing different environments in the two dimers because of the location of the linking disulfide bridge. In keeping with this interpretation, the Me18 chemical shifts (30.3, 30.5 ppm for wt; 30.4, 30.6 ppm for M23C−M23C; 30.3, 30.5 ppm for G51C−G51C) are not affected, because this group is facing the interior of the protein and is located further away from the engineered disulfide bridge.

Determination of Reduction Potentials. The midpoint potential determined for the wt protein by spectroelectrochemistry is 20 ± 5 mV (Table 1), a value close to those previously determined by spectroelectrochemistry (37 ± 5 mV) (*8*) and cyclic voltammetry (32 ± 5 mV) (present work). Similar values were obtained for the M23C and G51C monomers, indicating that the mutations by themselves did not affect the midpoint potential of the heme (Table 1). Cyclic voltammetry (CV) relies on the interaction of the ring of positive charges around the exposed heme edge of the protein with the negatively charged surface of the glassy carbon electrode. For this reason, the method could not be used

Table 1: Midpoint Potentials of Cytochrome *c*-553 Wild Type and Mutants M23C and G51C in Monomeric and Dimeric Forms[a]

sample	E_m (mV) cyclic voltammetry	sample	E_m (mV) spectroelectrochemistry
wt	32 ± 5	wt	20 ± 5
M23C	29 ± 5	M23C−M23C	88 ± 5
G51C	28 ± 5	G51C−G51C	105 ± 5

[a] All measurements were made at 20 °C in 50 mM potassium phosphate, pH 7.5.

for the homodimers where the masking of the ring of positive charges that are in proximity to the cysteine causes lack of interaction between the electrode surface and the protein.

This difficulty was overcome by exploiting the spectroelectrochemistry. The changes in the α- and *β*-bands of the absorption spectra were monitored as a function of potential in an anaerobic cuvette where the communication between the redox center and the working platinum electrode was facilitated by mediators free in solution. Under the experimental conditions used to determine the reduction potential of the wt protein, the reduction potential of the heme in M23C−M23C and G51C−G51C homodimers was found to be 88 ± 5 and 105 ± 5 mV, respectively (Table 1). Figure 4 shows the experimental points fitted to a single Nernst

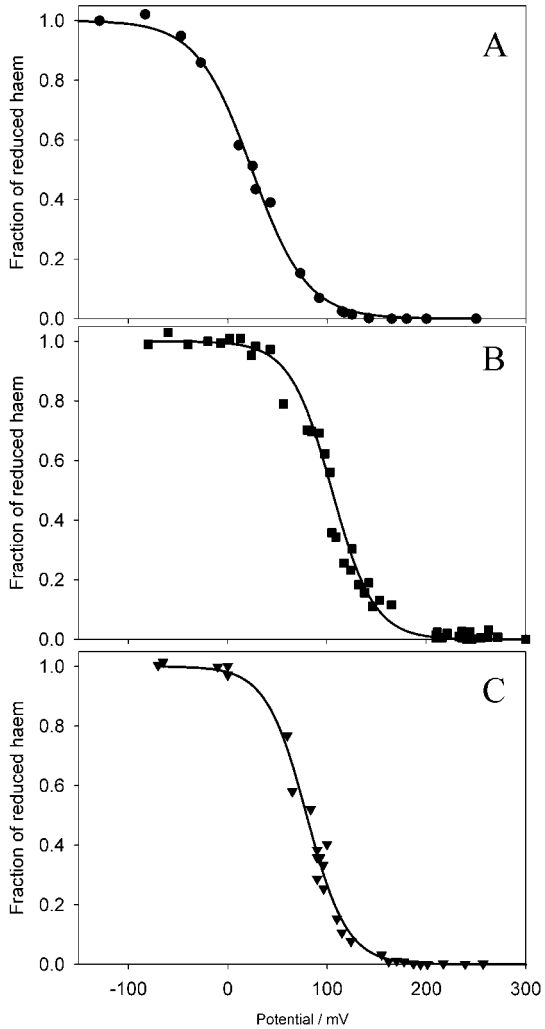

FIGURE 4: Spectroelectrochemical titration of cytochrome *c*-553 wt (A, circles), G51C−G51C (B, squares), and M23C−M23C (C, triangles). The solid lines represent the curves obtained by fitting of the data to the Nernst equation (eq 1).

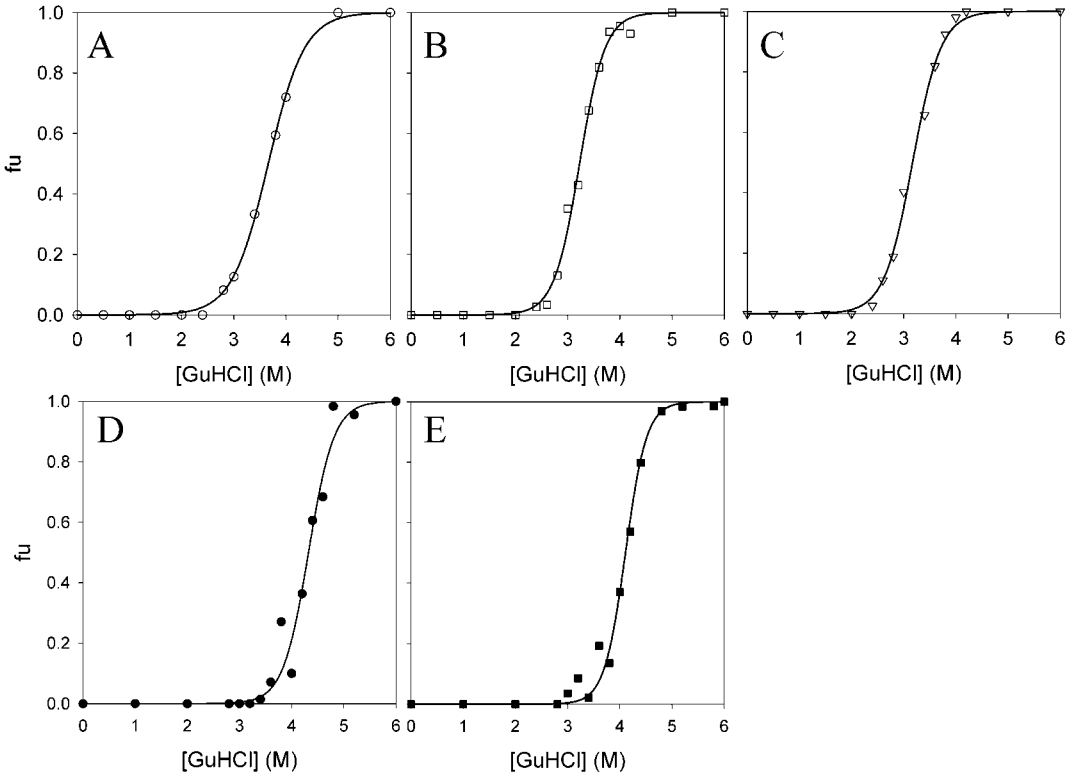

FIGURE 5: GuHCl-induced unfolding of oxidized (A, open circles) and reduced (D, filled circles) forms of *c*-553 wt, oxidized (B, open squares) and reduced (E, filled squares) G51C−G51C, and oxidized (C, open triangles) M23C−M23C, as monitored by far-UV CD. Conditions: 5 μM protein, 1 mm path length. Curves represent fitting assuming a two-state model.

curve considering the two hemes in the homodimers as two independent redox species. Both wt and G51C−G51C fitted curves resulted in an $n = 1 \pm 0.1$; the more scattered points of the M23C−M23C data set gave an $n = 1.2$ due to the error linked to the instability of the dimer under the reducing environment.

To ensure that the above-reported potentials belong to the native folded proteins, measurements were also performed in the presence of denaturing concentrations of GuHCl. In all of the denatured samples, the midpoint potential was found to be −80 mV, a value corresponding to denatured cytochrome *c* with the heme covalently attached to the unfolded polypeptide chain. In contrast to other cytochromes *c*, the heme in denatured cytochrome *c*-553 is pentacoordinated, not exhibiting the usual misligation in the sixth position. In the case of *c*-553, it has been shown that it retains the histidine ligand while no other ligand replaces the removed methionine (M57). Therefore, the iron is present in a high-spin form (*20*). In the present work, spectroscopic analysis (data not shown) confirmed the detachment of M57 in both the denatured monomeric and dimeric forms.

These data confirm that the shift of the reduction potentials toward higher values, observed in the native dimers, is indeed due to dimerization.

Thermodynamic Characterization. The behavior of oxidized and reduced cytochrome *c*-553 wild type and dimers in GuHCl was studied by far-UV CD spectroscopy. As shown by the results of Figure 5, the denaturation curves exhibit a single inflection point and a well-defined end point, consistent with a two-state model in which intermediate states are minimally populated at equilibrium. Dilution experiments, from high GuHCl concentration to buffer, indicated that the unfolding reaction is reversible. Both unfolding and refolding kinetics occurred in less than 1 min.

Table 2: Thermodynamic Parameters from the GuHCl-Induced Unfolding of Cytochrome *c*-553[a]

protein	ΔG^{H_2O} (kJ/mol)	$[GuHCl]_{1/2}$ (M)	*m* (kJ/mol)	n_B	ref
c-553$_{wt\ ox}$	26 ± 0.8	3.63	7.2 ± 0.1	31 ± 1	*b*
c-553$_{wt\ red}$	36 ± 3	4.31	8.4 ± 0.7	49 ± 4	*b*
M23C−M23C$_{ox}$	29 ± 1.2	3.14	9.3 ± 0.5	40 ± 3	*b*
G51C−G51C$_{ox}$	31 ± 1.2	3.22	9.8 ± 0.8	45 ± 3	*b*
G51C−G51C$_{red}$	49 ± 2	4.11	11.9 ± 0.5	59 ± 4	*b*
$c_{(horse)\ ox}$	40 ± 1	2.80	14.3 ± 0.4		*26*
$c_{(horse)\ red}$	74 ± 3	5.30	13.8 ± 0.4		*26*
$c_{(yeast)\ ox}$	24 ± 1	1.30	18.9 ± 0.5		*26*
$c_{(yeast)\ red}$	63 ± 3	3.80	16.6 ± 1.0		*26*
c-551$_{ox}$	34 ±	1.80	18.9 ± 42		*27*

[a] Data for horse (*26*), yeast (*26*), and *P. aeruginosa* (*27*) cytochromes *c* are included for comparison. $[GuHCl]_{1/2}$ indicates the GuHCl concentration at the midpoint of the unfolding transition, *m* is the molar cosolvent term, ΔG^{H_2O} is the free energy of unfolding in aqueous solution, and n_B is the apparent number of buried residues that become exposed upon unfolding. ox = oxidized; red = reduced. [b] This work.

The difference in Gibbs free energy in aqueous solutions ($\Delta G_{obs}^{H_2O}$), the molar cosolvent term (*m*), and the guanidinium chloride concentration at half-transition ($[GuHCl]_{1/2}$) were obtained on the basis of the linear extrapolation method (*16*), and the results are reported in Table 2. The difference in the free energies of the folded and unfolded states of the wt oxidized form is lower than those pertaining to the two oxidized homodimers by 3−5 kJ/mol.

The parameter *m* describes the steepness of the unfolding transition curve, and it has been assumed to be a measure of the hydrophobicity of the protein core (*21*). In the case of cytochromes, the heme will contribute extensively to the

hydrophobic core of the protein, and its solvent exclusion will contribute to the stability of the folded form. The *m*-value obtained for the wild type (7.2 kJ/mol), smaller than those obtained for the two homodimers (9.3−9.8 kJ/mol), is in agreement with a decreased solvent exposure of the heme as well as of residues at the interface between the two monomers (Table 2).

According to Staniforth (*18*), the cooperativity of protein denaturation can be correlated with the number of residues that become exposed to the solvent on unfolding. The "apparent" numbers of buried side chains (n_B) that were determined by fitting the experimental data to eq 6 are 31, 40, and 45 for the wt, the M23C−M23C dimer, and the G51C−G51C dimer, respectively. These numbers are apparent as they represent not only the actual numbers of residues but also the different exposure of the heme to the solvent in the native and in the denatured state of the protein. The increased value of n_B in the dimeric forms is consistent with the presence of an area, next to the disulfide bridge, at the interface between the two monomers, from which solvent has been excluded.

The ΔG values calculated from the denaturation curves suggest that the reduced forms of the homodimers and the wt monomer are more stable than the oxidized ones, as previously shown for other monomeric cytochromes by Winkler et al. (*22*). The comparison of the differences between the ΔG of denaturation of the oxidized and reduced forms of the wt and the G51C−G51C homodimer, 5 and 13 kJ/mol, respectively, shows that dimerization improves the stability of the reduced form more than that of the oxidized one. Changes in heme exposure may explain this behavior because the reduced/neutral form will be more affected by the water exclusion than the oxidized/charged one.

The comparison of the ΔG of unfolding of cytochromes *c* from different species (Table 2) shows that, within the oxidized forms, the ΔGs for unfolding are within 24−40 kJ mol^{-1} while, within the reduced forms, the ΔGs vary between 36 and 75 kJ mol^{-1}, in agreement with the increase in midpoint potential. This behavior has been interpreted in light of evolution (*20*), and it is interesting to observe that the trend observed upon formation of our engineered dimer is similar to that shown in natural cytochromes *c* from different species with decreasing heme exposure and increasing midpoint potential.

It has been shown (*20*, *22*) that the difference between the ΔG of denaturation of the oxidized and the reduced forms of several cytochromes matches the difference in midpoint potential between the native and the denatured states. Considering the thermodynamic cycle:

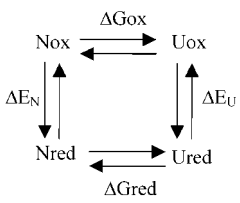

a good agreement exists between the $\Delta\Delta G$ values calculated from the difference in midpoint potentials between the native and denatured form, 12.5 kJ/mol for wt and 19.5 kJ/mol for G51C−G51C, and the $\Delta\Delta G$ values calculated between the ΔG of denaturation of the oxidized and the reduced form, 11.5 kJ/mol for wt and 18 kJ/mol for the G51C−G51C homodimer.

In the time scale of the denaturation experiments, the M23C−M23C dimer was found to split in monomers upon reduction. This phenomenon could be due to a specific reaction of sodium dithionite with a more highly reactive disulfide bond, possibly present in a stressed conformation. Because of this inconvenience the ΔG of denaturation of the reduced form of M23C−M23C homodimer could not be calculated.

On the basis of the observations in previous works (*8*, *10*, *23*, *24*), the increase in reduction potentials observed upon dimerization is due to two opposing contributions of enthalpy and entropy. Enthalpy changes have been shown to result from the interactions between heme and protein, including the solvent, and heme ligands. The entropy changes have been linked to differences in structural and solvation properties (*23*). In keeping with the observation that the entropic factor is playing a major role in changes in reduction potentials in *c*-553 (*8*, *10*), the increase in reduction potentials observed in this work is more likely to be due to entropy.

In conclusion, the data suggest that the differences in the *m*- and n_B-values and the stabilization of the reduced state and the reduction potentials show a trend consistent with the changes in accessible surface area of the heme between the monomeric and the dimeric forms. In the absence of the 3D structure, a model for the two homodimers was obtained by manual docking of the two mutants after insertion of the mutation in the 3D structure of the wt protein (Figure 1B). The Connolly algorithm using a probe of 1.4 Å radius (*25*) indicates a decreased heme exposure from 73 Å^2 for the wt to 66 and 50 Å^2 per heme for the M23C−M23C homodimer and G51C−G51C homodimer, respectively.

Experimental data and modeling are consistent and show the successful engineering of a cytochrome to raise its reduction potential. The data support the correlation between heme solvent accessibility and reduction potential and raise important questions on the actual reduction potentials in transient protein complexes forming in the course of biological electron transfer.

ACKNOWLEDGMENT

The authors thank Prof. Gerrit Voordouw (University of Calgary) for the generous gift of the pJRC41 plasmid and Dr. Steve Matthews (Imperial College) for the NMR experiments.

REFERENCES

1. Moore, G. R. (1996) in *Protein Electron Transfer* (Bendall, D. S., Ed.) pp 189−216, BIOS Scientific Publisher Ltd., Oxford.
2. Springs, S. L., Bass, S. E., and McLendon, G. L. (2000) *Biochemistry 39*, 6075−6082.
3. Shifman, J. M., Gibney, B. R., Sharp, R. E., and Dutton, P. L. (2000) *Biochemistry 39*, 14813−14821.
4. Kassner, R. J. (1972) *Proc. Natl. Acad. Sci. U.S.A. 69*, 2263−2267.
5. Churg, A., and Warshel, A. (1986) *Biochemistry 25*, 1675−1681.
6. Stellwagen, E. (1978) *Nature 275*, 73−75.
7. Tezcan, F., Winkler, J., and Gray, H. (1998) *J. Am. Chem. Soc. 120*, 13383−13388.
8. Bertrand, P., Mbarki, O., Asso, M., Blanchard, L., Guerlesquin, F., and Tegoni, M. (1995) *Biochemistry 34*, 11071−11079.
9. Blackledge, M. J., Guerlesquin, F., and Marion, D. (1996) *Proteins: Struct., Funct., Genet. 24*, 195−208.

10. Benini, S., Gonzalez, A., Rypiewski, W. R., Wilson, K. S., Van Beeumen, J. J., and Ciurli, S. (2000) *Biochemistry 39*, 13115−13126.
11. Blackledge, M. J., Medvedeva, S., Poncin, S., Guerlesquin, F., Bruschi, M., and Marion, D. (1995) *J. Mol. Biol. 245*, 661−681.
12. Valetti, F., Sadeghi, S. J., Meharenna, Y. T., Leliveld, S. R., and Gilardi, G. (1998) *Biosens. Bioelectron. 13*, 675−685.
13. Blanchard, L., Marion, D., Pollock, B., Voordouw, G., Wall, J., Bruschi, M., and Guerlesquin, F. (1993) *Eur. J. Biochem. 218*, 293−301.
14. Hagen, W. R. (1989) *Eur. J. Biochem. 182*, 523−530.
15. Dutton, P. L. (1978) in *Methods in Enzymology* (Fleisher, S., and Packer, L., Eds.) Vol. 54, pp 411−435, Academic Press, New York.
16. Shellman, J. A. (1987) *Biopolymers 26*, 549−559.
17. Santoro, M. M., and Bolen, D. W. (1988) *Biochemistry 27*, 8063−8068.
18. Staniforth, R., Burston, S., Smith, C., Jackson, G., Badcoe, I., Atkinson, T., Holbrook, J., and Clarke, A. (1993) *Biochemistry 32*, 3842−3851.
19. Senn, H., Guerlesquin, F., Bruschi, M., and Wuthrich, K. (1983) *Biochim. Biophys. Acta 748*, 194−204.
20. Wittung-Stafshede, P. (1999) *Protein Sci. 8*, 1523−1529.
21. Pace, N. C., Shirley, B. A., and Thomson, J. A. (1990) in *Protein structure: A practical approach* (Creghton T. F., Ed.) pp 311−330, IRL Press, Oxford, U.K.
22. Winkler, J., Wittung-Stafshede, P., Leckner, J., Malmstrom, B., and Gray, H. (1997) *Proc. Natl. Acad. Sci. U.S.A. 94*, 4246−4249.
23. Battistuzzi, G., Borsari, M., Sola, M., and Francia, F. (1997) *Biochemistry 36*, 16247−16258.
24. Battistuzzi, G., Borsari, M., Ranieri, A., and Sola, M. (2002) *J. Am. Chem. Soc. 124*, 26−27.
25. Connolly, M. L. (1983) *Science 221*, 709−713.
26. Mines, G. A., Pascher, T., Lee, S. C., Winkler, J. R., and Gray, H. B. (1996) *Chem. Biol. 3*, 491−497.
27. Bigotti, M. G., Allocatelli, C. T., Staniforth, R. A., Arese, M., Cutruzzola, F., and Brunori, M. (1998) *FEBS Lett. 425*, 385−390.

BI025759X